Reactive Power and AC Voltage Control of LCC HVDC System With Controllable Capacitors

Ying Xue and Xiao-Ping Zhang, *Senior Member, IEEE*

***Abstract*—It is well known that traditional line-commutated converter (LCC) based high voltage direct current (HVDC) system is not able to control its reactive power and terminal AC voltages. This paper investigates the reactive power and AC voltage control at the inverter side of the LCC HVDC system with controllable capacitors. The system's ability of operating under negative extinction angle is utilized to achieve a wide range of reactive power control and, in particular, the ability of exporting reactive power. In connection with the inverter AC terminal voltage or reactive power control, among different control possibilities at the rectifier side, active power control is desirable since large variations of active power transfer is very unfavorable. Detailed theoretical analysis is carried out first to show the reactive power controllability, and the capacitor voltage level is selected based on the desired control range. In addition, a new extinction angle measurement approach is proposed for negative extinction angle measurements. The effectiveness of the reactive power/voltage control capability for the proposed system is validated through simulation results using Real-Time Digital Simulator (RTDS). To verify the effectiveness of the reactive power and voltage control, CCC HVDC and LCC HVDC with SVC are also set up in RTDS, and simulation comparisons are made. Furthermore, contribution to AC voltage control in power system using the proposed method is demonstrated through simulation results of the modified two-area four-machine AC power system.**

***Index Terms*—AC voltage control, HVDC with controllable capacitor, HVDC transmission, LCC HVDC, reactive power control.**

I. Introduction

TRADITIONAL Line-Commutated Converter (LCC) based High Voltage Direct Current (HVDC) technology has played an important role in long distance bulk power transmission around the world since its first application 60 years ago. However some well-known limitations associated with it still exist today which to a certain extent limit further applications of such a technology. One of the limitations is significant reactive power requirement at both sides of the HVDC system. The reactive power requirement originates from the firing of thyristors after commutation voltage becomes positive, which in effect delayed the current waveforms with respect to the voltage waveforms [1]. So both rectifier and inverter sides of the system absorb reactive power. However it should be noted that to the sending end AC system, the rectifier represents a load and it is natural that it draws some reactive power from the network just like other loads. On the other hand, from the point of view of the receiving end AC system, the inverter acts as a power producer and as such should take its share of reactive load. But the reality is that instead of producing, the inverter consumes reactive power thus its consumption level of reactive power should be minimized. Furthermore, with passive reactive power compensation at the inverter side, the level of reactive power being produced tends to decrease under transient AC voltage drops when reactive power support is needed most. At the same time, the minimum extinction angle controller will advance its firing angle which leads to a higher reactive power consumption and causes further AC voltage drops. These operational characteristics are clearly unfavorable, and FACTS devices such as STATCOM and static var compensator (SVC), etc. may be needed to mitigate the problem.

In contrast to what has been described above, the desired inverter performances can be listed as follows:

- Very low or zero reactive power consumption level at steady-state.
- AC voltage control by inverter itself especially under large AC disturbances.

It should be pointed out that the reactive power or voltage controllability at the inverter side should not be achieved at the expense of reduced active power transfer level, as the primary role of an HVDC link is to provide a stable active power transfer. In this way, the advantage of the inverter reactive power control can be maximized.

For a back-to-back LCC HVDC scheme it is possible to design reactive power controller at the inverter side to control its reactive power consumption [2], [3]. In this case since the two converter stations are located on the same site, the problems of communication delay and the risk of loss of communications between rectifier and inverter control systems are minimized. Also the measurements from both terminals are readily available for both control systems. Hence it is possible for the inverter to control its reactive power consumption by varying its extinction angle while the danger of losing commutation margin can be mitigated by the rectifier controller modifying its operating conditions. This type of control helps improve the AC voltage stability at the inverter bus by controlling reactive power consumption, but considerable steady state reactive power consumption still remains. In addition this type of control strategy is limited to back-to-back HVDC schemes.

For point to point HVDC schemes, unlike back-to-back schemes, the communication delay and/or the requirements for the system to operate without communications largely limit

Manuscript received December 5, 2015; revised March 15, 2016; accepted April 19, 2016. Date of publication May 5, 2016; date of current version December 20, 2016. This work was supported by EPSRC under Grant EP/L017725/1. Paper no. TPWRS-01743-2015.

The authors are with the Department of Electronic, Electrical and Systems Engineering, University of Birmingham, Birmingham B15 2TT, U.K. (e-mail: xue237039454@gmail.com; x.p.zhang@bham.ac.uk).

Color versions of one or more of the figures in this paper are available online at http://ieeexplore.ieee.org.

Digital Object Identifier 10.1109/TPWRS.2016.2557342

the possibility of reactive power control. Most of the literatures are then focused on reactive power compensation rather than reducing reactive consumption level of converter [4]–[12]. In those methods, external reactive compensation devices are installed at the inverter AC side. It is well known that a LCC inverter could not control its reactive power consumption because the extinction angle cannot be desirably small in order to ensure sufficient commutation margin in case of disturbances on the inverter AC side. Hence, various methods of managing and optimizing the externally installed reactive compensation devices have been investigated so as to support the operation of the LCC Inverter [13]–[15].

One of the promising methods which can operate with better power factor angle is the Capacitor Commutated Converter (CCC) based HVDC [16]–[20]. Depending on the size of capacitors, the phase shift introduced by these capacitors to the valve side commutation voltage can be such that the inverter side is able to achieve around 10%–15% reactive power consumption. However this usually requires large capacitors which significantly increase valve voltage stress and costs [21].

This paper focuses on achieving the aforementioned desired inverter performances by further exploiting the reactive power control capability of the previously proposed LCC HVDC system with controllable capacitors [22]. Since capacitor insertions change the dynamic behavior of the inverter, theoretical analysis need to be carried out to investigate the reactive power controllability. The effects of capacitor insertions have on the system variables are calculated for the first time. Then the inverter power factor as a function of extinction angle is calculated and is used to demonstrate the controllability. Finally with theoretical analysis as the basis, controllers are designed to validate the reactive power and AC voltage control performances.

The rest of the paper is organized as follows. Section II briefly reviews the system configuration and explains its operational concepts. Section III analytically derives how reactive power is related to other system variables. Section IV presents the proposed extinction angle measurement, the designed reactive power controller and inverter AC voltage controller. Section V firstly shows the simulation results of reactive power control and inverter AC voltage control, respectively, of the proposed system using the modified CIGRE benchmark system. Comparisons with CCC HVDC are made. Then the simulation results of applying the proposed method in two-area four-machine system are presented. After that further comparisons with LCC HVDC with SVC are made. All simulations are carried out using real time digital simulator (RTDS). Finally concluding remarks are given in Section VI.

II. System Configuration and Operational Concepts

A. System Configuration

The LCC HVDC system with controllable capacitors [22] and the connected AC system at the inverter side are shown in Fig. 1. In the figure, *TY1-TY6* and *TD1-TD6* are thyristor valves, *CapYa*, *CapYb*, *CapYc* and *CapDa*, *CapDb*, *CapDc* are capacitor modules, *S1Ya-S4Ya* are four insulated gate bipolar transistor (IGBT) switches for capacitor module *CapYa*. The

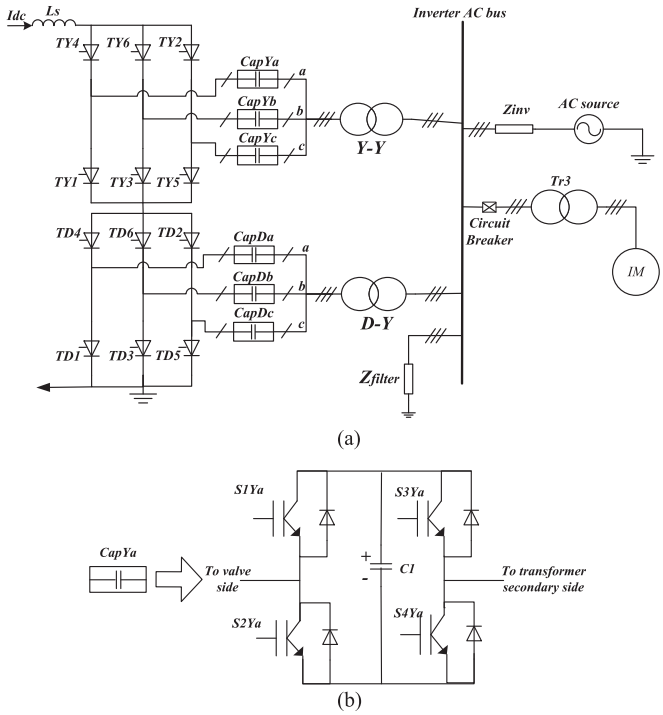

Fig. 1. Configuration of LCC HVDC system with controllable capacitors. (a) Inverter and connected AC system. (b) Capacitor module configuration.

system is based on the CIGRE HVDC Benchmark model with all the system parameters got from [23]. An induction machine is added to the inverter AC bus to test the AC voltage controller performance. Capacitor modules are connected in series between the secondary side of converter transformers and thyristor valves. Each capacitor module can be realized by a single module (as that for 2-level VSC) or by a number of series connected sub-modules to achieve higher insertion voltage. Each module consists of four IGBT switches with anti-parallel diode across each one of them. The reference polarity of the capacitor is shown in Fig. 1(b). Each capacitor module will be inserted as a positive voltage when *S1* and *S4* are switched on and *S2* and *S3* are switched off, and will be inserted as a negative voltage when *S2* and *S3* are switched on and *S1* and *S4* are switched off. Bypass is achieved by switching *S1* and *S3* on or *S2* and *S4* on at the same time.

B. Insertion Strategy

The so called ‘push’ & ‘pull’ insertion strategy works by inserting capacitor modules into the two commutating phases during commutation. The polarities of the inserted capacitors are such that the voltages provided by them are in favor of the commutation process. For example for the commutation from *TY2* to *TY4* as shown Fig. 2, *CapYc* is inserted as a positive voltage and *CapYa* is inserted as a negative voltage until the commutation is complete. *CapYb* in phase B is in bypass mode during this commutation process. This additional commutation voltage from the inserted capacitors guarantees the successful commutations when inverter is exporting reactive power. It should be mentioned that compared with CCC

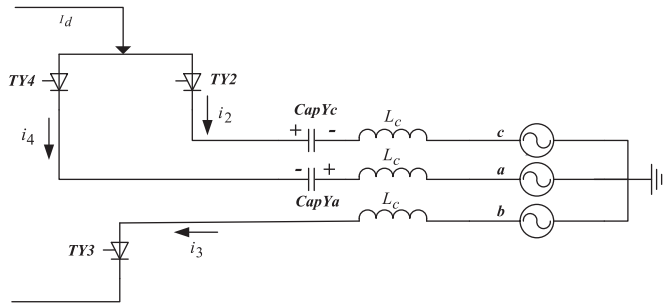

Fig. 2. Commutation from TY2 to TY4.

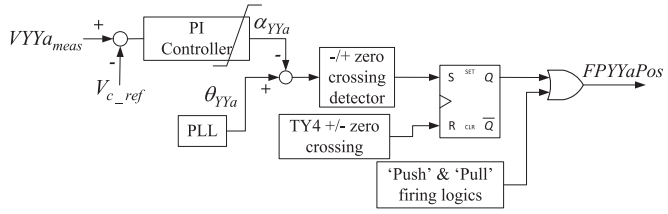

Fig. 3. Capacitor voltage balancing logics.

HVDC, since the controllable capacitors are mainly inserted into the circuit during commutation period, valve voltage stress is slightly increased, and is comparable to the original LCC HVDC system [22].

C. Capacitor Voltage Balancing

The balancing of capacitors takes place when one of the two thyristor valves connected to that specific phase is conducting. Considering the balancing of *CapYa*, it can be charged or discharged when *TY4* or *TY1* is fully conducting. The designed balancing strategy inserts *CapYa* as a positive voltage before the firing of *TY6* and bypasses it when the commutation from *TY4* to *TY6* is complete. The main control logics for *CapYa* balancing are shown in Fig. 3 where $VYYa_{\rm meas}$ and V_{c_ref} are the measured and reference values for *CapYa* voltage, $\theta_{\rm YYa}$ is the phase reference for actual insertion time and *FPYYaPos* is the switching word. It can be seen that the control angle $\alpha_{\rm YYc}$ at which *CapYa* is inserted is generated by minimizing its voltage error signal through a PI controller. The actual switching word $FPYYaPos$ is determined by comparing the control angle with the relevant phase information from PLL. The voltage balancing logics of all the other capacitor modules have the similar structure but with different phase information. It is worth mentioning that for the CCC HVDC where capacitor voltages are not controlled, unbalanced capacitor voltages can appear during unbalanced faults. This can add additional complexity to the control system. However for the proposed system where capacitor voltages are actively controlled, they can stay balanced during unbalanced fault, and therefore reduce the complexity of control system.

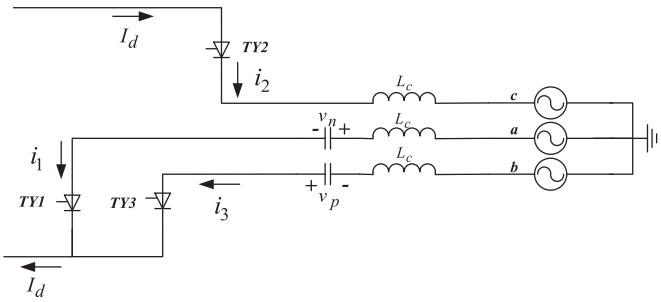

Fig. 4. Commutation from TY1 to TY3.

III. Theoretical Analysis of Reactive Power Controllability

This section is to examine the reactive power controllability by capacitor insertion and firing angle control. The capacitor insertion strategy and capacitor voltage balancing actions affect the system from three different aspects. Firstly the overlap angle is smaller due to additional commutation voltage from capacitors. Secondly the average voltage across the 6-pulse bridge is increased due to the difference of capacitor voltage change during commutation. Thirdly the pre-insertion of capacitors for charging purpose also increases the average bridge voltage. In the following, analytical derivations will be presented for all three aspects and then variation of power factor (interchangeably variation of reactive power) as a function of firing angle and extinction angle will be shown. In addition, selection of capacitor voltage level for the desired operating range is also presented.

A. Commutation Overlap

The commutation period from *TY1* to *TY3* as shown in Fig. 4 is considered in this section where L_c is the transformer leakage inductance, C is the capacitor value, v_n is the instantaneous voltage for the capacitor inserted in negative direction and v_p is the instantaneous voltage for the capacitor inserted in positive direction, i_1 and i_3 are instantaneous currents flowing through *TY1* and *TY3,* respectively. The instantaneous line-to-neutral source voltages are

$$\begin{aligned} e_a &= E_m \cos(\omega t + 60^o) \\ e_b &= E_m \cos(\omega t - 60^o) \\ e_c &= E_m \cos(\omega t - 180^o) \end{aligned} \tag{1}$$

where E_m is the phase voltage magnitude and ω is the rated system angular frequency. Dynamic equations for the commutation loop can be written as [22]

$$i_1 + i_3 = I_d \tag{2}$$

$$i_1 = C\frac{dv_n}{dt} \tag{3}$$

$$i_3 = -C\frac{dv_p}{dt} \tag{4}$$

$$e_b - L_c\frac{di_3}{dt} + v_p = e_a - L_c\frac{di_1}{dt} - v_n. \tag{5}$$

With initial conditions

$$v_p(t)|_{t=\alpha/\omega} = V_o \tag{6}$$

$$\frac{dv_p(t)}{dt}|_{t=\alpha/\omega} = -\frac{1}{C} i_3|_{t=\frac{\alpha}{\omega}} = 0 \tag{7}$$

where α is the firing angle and $V_o$is the initial charged capacitor voltage. By solving (2)–(5), $v_p$and $i_3$can be obtained as follows [22]:

$$v_p = C_1 \cos\omega_n t + C_2 \sin\omega_n t + B\sin\omega t + D \tag{8}$$

$$i_3 = -C(-C_1\omega_n \sin\omega_n t + C_2\omega_n \cos\omega_n t + B\omega\cos\omega t - \frac{I_d}{2C}) \tag{9}$$

where

$$C_1 = aV_0 - Ba\sin\alpha - \frac{bI_d}{2\omega_n C} + \frac{Bb\omega}{\omega_n}\cos\alpha \tag{10}$$

$$C_2 = bV_0 - Bb\sin\alpha + \frac{aI_d}{2\omega_n C} - \frac{Ba\omega}{\omega_n}\cos\alpha \tag{11}$$

$$a = \cos\frac{\omega_n}{\omega}\alpha \tag{12}$$

$$b = \sin\frac{\omega_n}{\omega}\alpha \tag{13}$$

$$\omega_n = \frac{1}{\sqrt{L_c C}} \tag{14}$$

$$B = \frac{-\sqrt{3}E_m}{2L_c C} \times \frac{1}{\omega_n^2 - \omega^2} \tag{15}$$

$$D = -\frac{I_d}{2C}t + \frac{I_d\alpha}{2\omega C}. \tag{16}$$

Since at the end of commutation $t = \frac{\alpha+\mu}{\omega}$ and $i_3 = I_d$ (where μ is the overlap angle),

$$I_d - C - \left(C_1\omega_n \sin\omega_n\frac{\alpha+\mu}{\omega} + C_2\omega_n\cos\omega_n\frac{\alpha+\mu}{\omega} + B\omega\cos\omega\frac{\alpha+\mu}{\omega} - \frac{I_d}{2C}\right). \tag{17}$$

Using the parameters from Benchmark model and C of 585 μF, overlap angle μ can be calculated as a function of capacitor voltage levels for different firing angles by solving (17). The capacitor value of 585 μF is the same as that calculated in [22] so that the level of capacitor voltage change is not significant after each commutation. It can be seen from Fig. 5 that as capacitor voltage increases, overlap angle reduces to about10^0 and does not vary significantly for different firing angles.

B. Pre-Insertion of Capacitors

The duration of pre-insertion of capacitors depends on the level of its voltage reduction over a cycle. For the same commutation period from *TY1* to *TY3*, the voltage increase in the outgoing phase is

$$\Delta V_{\text{in}} = v_n\left(\frac{\alpha+\mu}{\omega}\right) - V_0 \tag{18}$$

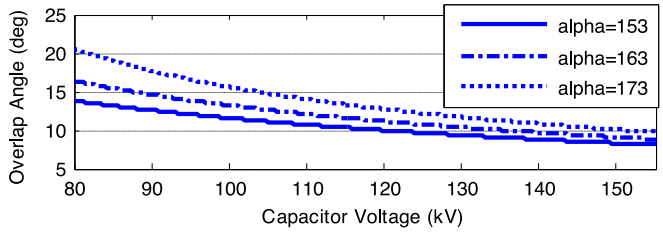

Fig. 5. Variation of overlap angle against capacitor voltage for different firing angles.

and the voltage decrease in the incoming phase is

$$\Delta V_{\text{de}} = V_0 - v_p\left(\frac{\alpha+\mu}{\omega}\right). \tag{19}$$

By substituting (3) and (4) into (2) and then integrate over the whole commutation period gives

$$v_n\left(\frac{\alpha+\mu}{\omega}\right) = v_p\left(\frac{\alpha+\mu}{\omega}\right) + \frac{I_d\mu}{\omega C}. \tag{20}$$

Since for one cycle each capacitor voltage increases and decreases two times so the net decrease of voltage is

$$\Delta V_{\text{total}} = 2\Delta V_{\text{de}} - 2\Delta V_{\text{in}}. \tag{21}$$

Substituting (18)–(20) into (21),

$$\Delta V_{\text{total}} = 4V_0 - 4v_p\left(\frac{\alpha+\mu}{\omega}\right) - \frac{2I_d\mu}{\omega C}. \tag{22}$$

Hence the pre-insertion time required per cycle is

$$\Delta t = \frac{\Delta V_{\text{total}} \times C}{I_d}. \tag{23}$$

Therefore the average voltage increase due to the pre-insertion of capacitor is

$$\Delta V_{\text{pre}} = \frac{V_0 \times \Delta V_{\text{total}} \times \omega C}{2\pi I_d}. \tag{24}$$

C. Commutation

For the same commutation period from *TY1* to *TY3*, the bridge lower point voltage during commutation is

$$V_{\text{low}} = \frac{(e_a - v_n) + (e_b + v_p)}{2}. \tag{25}$$

So the average voltage increase over a cycle due to the bridge voltage increase during commutation is

$$\Delta V_\mu = \left[\int_{\frac{\alpha}{\omega}}^{\frac{\alpha+\mu}{\omega}} \frac{e_a + e_b}{2}dt - \int_{\frac{\alpha}{\omega}}^{\frac{\alpha+\mu}{\omega}} \frac{(e_a - v_n) + (e_b + v_p)}{2}dt\right] \Big/ \left(\frac{\pi}{3}\right). \tag{26}$$

Considering (2)–(3), (26) can be simplified to

$$\Delta V_\mu = \frac{3\mu^2 I_d}{4\pi\omega^2 C}. \tag{27}$$

Similar to (24), ΔV_μ can be calculated once overlap angle is solved.

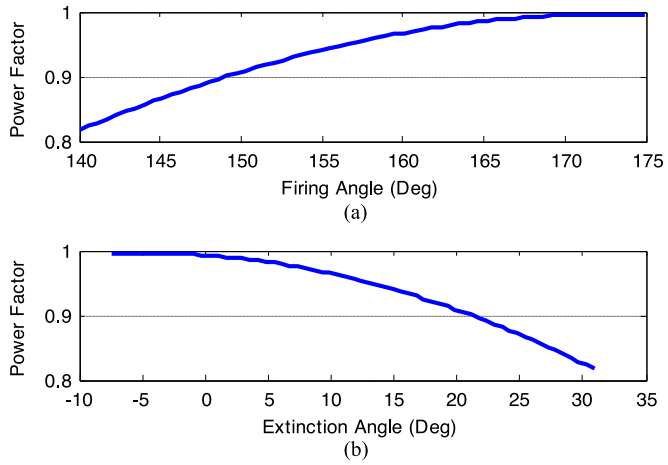

Fig. 6. Variation of power factor against different control variables. (a) Powerfactor against firing angle. (b) Power factor against extinction angle.

D. Power Factor

Without capacitor insertions the average DC voltage is given by

$$V_{\text{original}} = \frac{3\sqrt{6}}{\pi}\frac{\cos(\alpha)+\cos(\alpha+\mu)}{2}E_{\text{LN}} \tag{28}$$

where E_{LN} is the RMS line-to-neutral voltage.

Hence the average DC voltage with capacitor insertions is

$$V_d = |V_{\text{original}}| + \Delta V_{\text{pre}} + \Delta V_{\mu}. \tag{29}$$

The absolute value is used since DC voltage calculated using (28) is negative at inverter side. If losses are neglected, AC power and DC power are equal:

$$3E_{\text{LN}} I_{L1} \cos\phi = V_d I_d \tag{30}$$

where I_{L1} is the RMS fundamental frequency current and $\cos\phi$ is the power factor. It is well known that I_{L1} can be approximated by fundamental frequency current when overlap angle is zero

$$I_{L1} = \frac{\sqrt{6}}{\pi} I_d. \tag{31}$$

The approximation is quite accurate given the normally much smaller overlap with the proposed system. Finally by substituting (29) and (31) into (30), power factor for the proposed system can be calculated as

$$\cos\phi = \frac{\pi V_d}{3\sqrt{6}E_{\text{LN}}}. \tag{32}$$

Fig. 6 shows the variation of power factor as a function of firing angle and extinction angle, and this means that reactive power at the inverter AC side can be controlled via the firing angle. In particular by controlling the firing angle to be close to 180°, power factor can be favorably controlled to be about unity. At the same time as shown in Fig. 6(b), the extinction angle is negative which means that commutation completes after the AC commutation voltage becomes negative. The success of commutation in this case is guaranteed by the commutation voltage from the capacitors. Also it motivates the design of new method of extinction angle measurement to accommodate negative values since the traditional method usually output zero extinction angles when commutation process stretches after voltage zero crossing point.

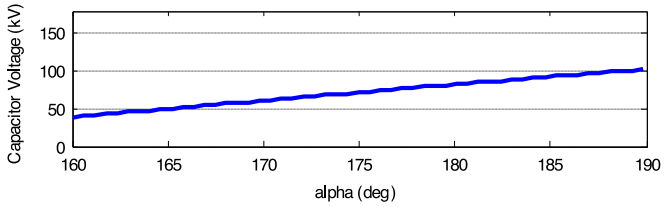

Fig. 7. Required capacitor voltage for a range of firing angles.

E. Capacitor Voltage Level

The required capacitor voltage level is determined by the desired operating range. In this design, the nominal operating condition of inverter side is at unity power factor which means a firing angle close to 180°, so a maximum firing angle of 190° is chosen for the selection of capacitor voltage level.

If the maximum overlap angle is chosen to be$\mu_{\max} = 40^\circ$ for safe commutation, the necessary condition for successful commutation is

$$i_3|_{t=\frac{\alpha+\mu_{\max}}{\omega}} \geq I_d \tag{33}$$

where firing angle α is varying and has a maximum value of 190°.

By solving (33) using (9) for a range of firing angles, the required capacitor voltage level can be obtained. Fig. 7 shows the required voltage level with firing angle ranges from 160° to 190°. It should be noted that in this case the normal operating point is at unity power factor which means a higher AC voltage, hence the transformer turns ratio is modified to achieve the same power transfer level at similar DC and AC voltages as the original benchmark system. From the calculated results in Fig. 7, capacitor voltage level of 110 kV is chosen for simulation studies.

IV. Reactive Power and AC Voltage Control

A. Extinction Angle Measurement

Traditionally, extinction angle for a specific thyristor valve is obtained by measuring the time between the completion of commutation and the point when valve voltage becomes positive. However with the proposed system, inverter side can have the ability to export reactive power which means the extinction angle can sometimes be negative. Consequently new method of extinction angle measurement with the ability to accommodate negative values is needed. In this paper, such a method is proposed which can be explained with reference to Fig. 8 which shows the measurement of extinction angle for *TY2*. A pulse *Q* is generated when commutation voltage e_{ca} becomes positive and is reset when *TY2* current reaches zero. Then by subtracting the phase angle represented by the length of *Q* from 180°, extinction angle for *TY2* can be calculated. The final measured extinction angle for the control system is obtained by taking

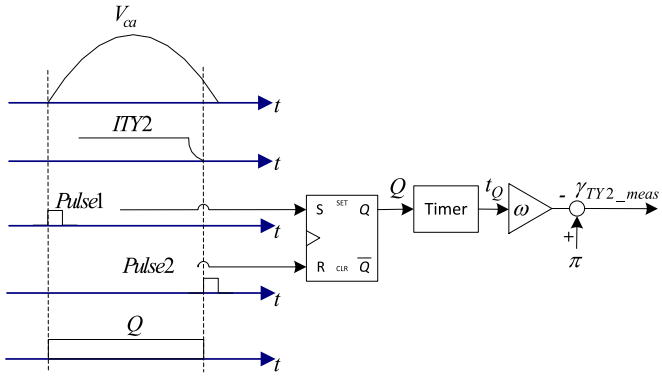

Fig. 8. Proposed extinction angle measurement for TY2.

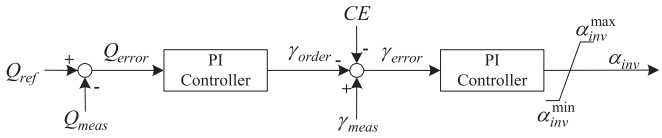

Fig. 9. Proposed inverter reactive power controller.

the minimum of all the calculated extinction angles for all the valves. In this way, negative extinction angle can be measured which enables the design of reactive power feedback controller.

B. Reactive Power Controller

From theoretical analysis, it can be seen that reactive power can be favorably controlled. Since the original inverter side is using minimum extinction angle control, the reactive power controller can be designed as such that the extinction angle order is generated by an outer reactive power control loop rather than a constant. Fig. 9 shows the proposed reactive power controller at inverter side where $Q_{\rm ref}$, $Q_{\rm meas}$ and $Q_{\rm error}$ are reactive power reference, measurement and error signals, respectively; $\gamma_{\rm order}$, $\gamma_{\rm meas}$ and $\gamma_{\rm error}$ are extinction angle order, measurement and error, respectively; *CE* is the inverter current error signal and $\alpha_{\rm inv}$ is the inverter firing angle. It can be seen that extinction angle reference is generated by minimizing the reactive power error by a PI controller. Ideally the extinction angle order can be calculated from reactive power reference based on equations from Section III. However due to the highly nonlinear relationship between extinction angle and reactive power, PI controller is applied. Note that since the extinction angle measurement can be negative, the controller is able to control the inverter terminal to export reactive power if needed.

C. AC Voltage Controller

To control the AC voltage at the inverter AC bus, an AC voltage controller can be designed utilizing the reactive power controllability of the proposed system. In this case, the AC voltage is controlled by controlling the reactive power import/export of the inverter station. Therefore the inverter AC voltage stability can be improved. The proposed inverter controller is shown in Fig. 10 where $V_{\rm ref}$ and $V_{\rm meas}$ are inverter AC voltage reference and measured values, respectively. As can be seen from Fig. 10, a PI controller is used to generate inverter firing angle by minimizing AC voltage error.

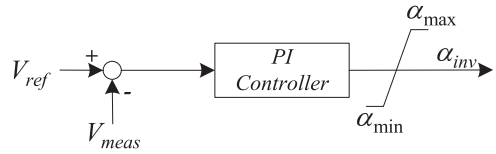

Fig. 10. Proposed Inverter AC voltage controller.

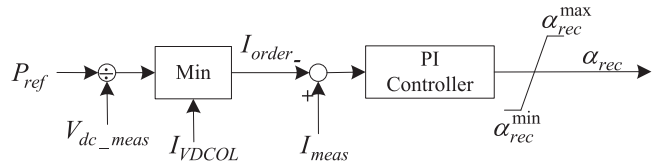

Fig. 11. Rectifier active power controller.

D. Rectifier Active Power Control

As discussed before that it is important to ensure that active power transfer of the DC system is kept at desired values when inverter is controlling reactive power/AC voltage. Such operational behavior is achieved by utilizing rectifier side controller to control active power transfer. Fig. 11 shows the active power controller being applied at rectifier side. The active power reference $P_{\rm ref}$ is divided by DC voltage measurement $V_{\rm dc\_meas}$ to get the desired current, and the DC current order signal $I_{\rm order}$ is obtained by taking the minimum value of desired current and current order from VDCOL-$I_{\rm VDCOL}$. Finally PI controller is used to generate the control input of firing angle $\alpha_{\rm rec}$.

The parameters for the above PI controllers are selected by trial and error through simulation studies.

V. Simulation Results

This section presents the simulation results of reactive power control and inverter AC voltage control of the LCC HVDC system with controllable capacitors. The nominal operating point for both cases is designed so that the inverter side is absorbing zero reactive power and sending rated active power at rated DC and AC voltages. The capacitor banks are removed and transformer turns ratio is modified to meet the rated working condition. The values of capacitors are $585\ \mu$F and its voltage level is chosen to be 110 kV. The rectifier side is controlling the active power transfer by controlling the DC current. The AC systems at both sides are kept the same as the CIGRE HVDC benchmark model. The whole system is modelled in RTDS with a small simulation time-step of $3.6\ \mu$s.

A. Reactive Power Control

Fig. 12 shows the system responses following changes of reactive power reference. In this simulation, the reactive power reference is initially set to zero and changes to –150 MVar at 3.1 s, then increases to 150 MVar at 4.6 s and finally changes

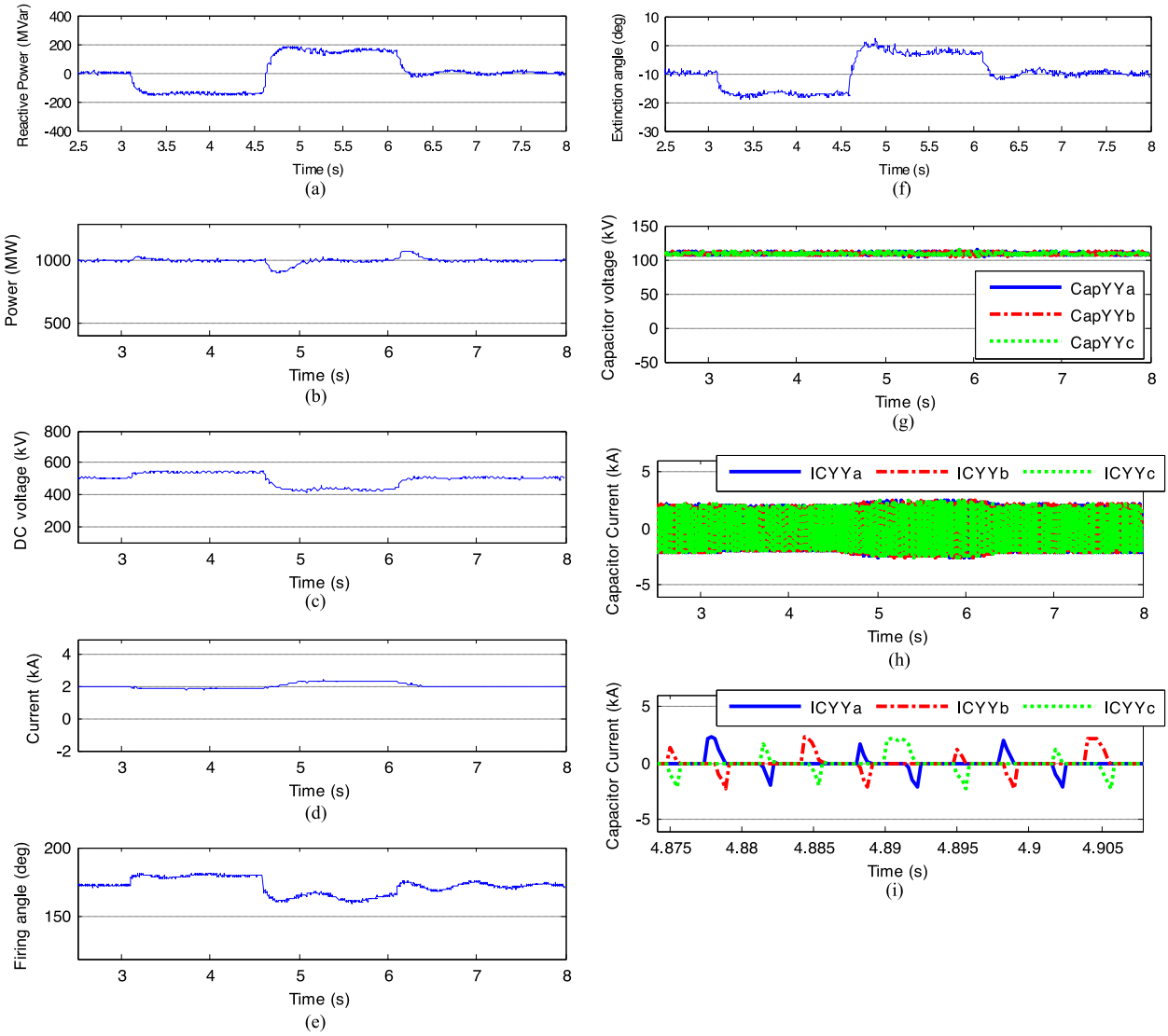

Fig. 12. System responses with reactive power reference step changes. (a) Reactive power consumption at inverter. (b) Active power transfer. (c) DC voltage. (d) DC current. (e) Inverter firing angle. (f) Extinction angle. (g) Capacitor voltages (CapYYa, CapYYb, CapYYc). (h) Capacitor currents for CapYYa, CapYYb and CapYYc. (i) Zoomed in version of capacitor currents.

back to zero at 6.1 s. Negative reactive power indicates that the inverter is exporting reactive power to the AC system.

It can be seen from Fig. 12(a) that measured reactive power successfully tracks the reference and is able to achieve zero steady-state reactive power consumption. It can also be observed that inverter can export reactive power if needed. At the same time, active power transfer on the DC link is controlled at the rated value which is shown in Fig. 12(b). The response of the DC active power at the instants of step changes of the reactive power can be explained by considering controller actions. For example when the reactive power reference is increased, the inverter firing angle is decreased according to the controller shown in Fig. 9. This decrease of inverter firing angle leads to a decrease of the DC voltage. Therefore the DC power drops transiently as the DC current cannot be changed instantly. Similarly when the reactive power reference is decreased, there is a transient increase of the DC active power. Since the change of the reactive power is achieved by modifying the firing angles, the DC voltage also changes. Both the inverter firing angle and the DC voltage are shown in Fig. 12(e) and (c). Fig. 12(d) shows that the DC current is slightly changed to keep a constant active power level and in Fig. 12(f) the corresponding changes in extinction angle are shown. Negative values of the extinction angle validate the effectiveness of the proposed method to measure the negative extinction angle. The success of commutations with a negative extinction angle is due to the additional commutation voltages from the inserted capacitors [22]. Finally the voltage and current for the controllable capacitors throughout the simulation period are shown in Fig. 12(g) and (h), respectively. From Fig. 12(g) it can be seen that the capacitor voltages are well balanced by the capacitor voltage controller. Fig. 12(i) is the zoomed in version of Fig. 12(h) which shows how the capacitor currents charge and discharge the capacitors.

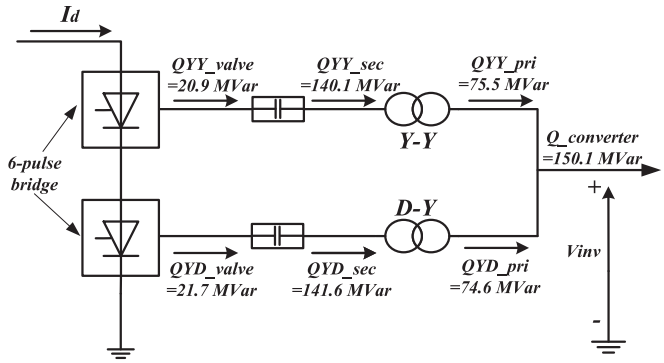

Fig. 13. Reactive power flow distribution when the inverter is exporting reactive power.

To further illustrate the reactive power flow distribution when the inverter is exporting reactive power, Fig. 13 is included where the inverter is controlled to export 150 MVar of reactive power. In Fig. 13, *QYY_valve* and *QYD_valve* are reactive power flows between the valve side and controllable capacitors for upper and lower 6-pulse bridges, respectively; *QYY_sec* and *QYD_sec* are the reactive power flows between the secondary side of converter transformer and controllable capacitor for the upper and lower 6-pulse bridges, respectively; *QYY_pri* and *QYD_pri* are the reactive power flows at primary side of converter transformer for the upper and lower 6-pulse bridges, respectively; *Q_converter* is the total inverter reactive power output; I_d is the DC current; $V_{\rm inv}$ is the inverter AC bus voltage. The values shown in Fig. 13 are the averaged reactive power flows. It can be seen that in this case both 6-pulse bridges are exporting reactive power. This is because the fundamental component voltage lags the fundamental component current when the extinction angle is negative. This export of reactive power is then increased by the reactive power generated from the controllable capacitors. Finally the net reactive power export of the inverter is obtained by including the transformer reactive power consumption.

B. AC Voltage Control

This case study is used to demonstrate the inverter AC voltage controllability following large inductive load changes. The inverter side is using the proposed AC voltage controller. The load being considered in this case study is an induction machine with a rating of 98.5 MVA and a power factor of 0.94. It is connected to the inverter AC bus and is switched in and out by controlling the connected circuit breakers.

Fig. 14 shows the simulation results when an induction machine is switched in at 0.4 s. It can be seen from Fig. 14(d) that induction machine draws significant amount of reactive power once switched in to the system. It causes a transient AC voltage drop as shown in Fig. 14(a). The inverter controller then quickly increases its firing angle (see Fig. 14(f)) to compensate the extra reactive power requirement to bring back the AC voltage. As a result, the inverter starts to export reactive power which is shown in Fig. 14(b). At the same time, the active power transfer level on the DC link is controlled by the rectifier power controller as shown in Fig. 14(c). Similar to the previous case study, both the voltage and current for the controllable capacitors are shown in Fig. 14(g) and (h), respectively. Fig. 14(g) shows that the capacitor voltages are successfully controlled at the reference value throughout the simulation period. Similar to Fig. 12(i), Fig. 14(i) shows the zoomed in version of capacitor currents (see Fig. 14(h)) which charge and discharge the capacitors during commutation periods.

In order to verify the results and to further demonstrate the system's reactive power controllability, responses from CCC HVDC system subject to the same switching scenario are presented. The CCC HVDC system being used for this case study is established by modifying the CIGRE benchmark model by adding fixed series capacitors of $92.6\ \mu$F. Also the reactive power support from the filter banks are modified to compensate about 15% of the active power transfer level at rated condition. Under normal operating condition, the apparent extinction angle $\gamma_{\rm app}$ is about 2°, which corresponds to an actual extinction angle of about 27°. The above settings for CCC HVDC agree with those from literatures [20], [24], [25]. The same rectifier and inverter controllers are employed for better comparison.

Simulation results are shown in Fig. 15. It can be seen that when the induction machine is switched in and brings down the inverter AC voltage, the inverter firing angle is increased trying to provide reactive power support as shown in Fig. 15(c). However, the system is not able to produce sufficient reactive power to bring the AC voltage back, and fails to work. The DC side voltage collapses to zero and DC current increases significantly which can be observed from Fig. 15(d) and (e), respectively. The large DC current charges the fixed series capacitors and causes significant increase of inverter AC bus voltage as shown in Fig. 15(a). In practical systems, the DC system will be blocked under such circumstances to limit the overvoltage and overcurrent. However for the purpose of comparison of dynamic responses of the systems, the associated protection actions are not simulated.

C. Dynamic Performance of a Two-Area Four-Machine AC Power System With the LCC HVDC With Controllable Capacitors

In order to show how the proposed method contributes to power system dynamics, simulation studies of AC voltage control using the LCC HVDC system with controllable capacitors in the well-known two-area four-machine system [1] are carried out. For the sake of comparisons, simulation studies of applying the HVDC benchmark system in the same two-area four-machine system are also carried out. The single-line diagrams of both systems are shown in Fig. 16. It can be seen from Fig. 16 that one of the AC transmission lines between bus 7 and bus 9 is replaced with the HVDC link in both systems. In addition, the active power load at bus 7 and bus 9 are modified for both systems so that each line between the two buses transmits 250 MW of active power under steady state condition. The active power control references of both the HVDC systems are modified to 250 MW accordingly. The inverter side of the proposed system is controlling the AC voltage

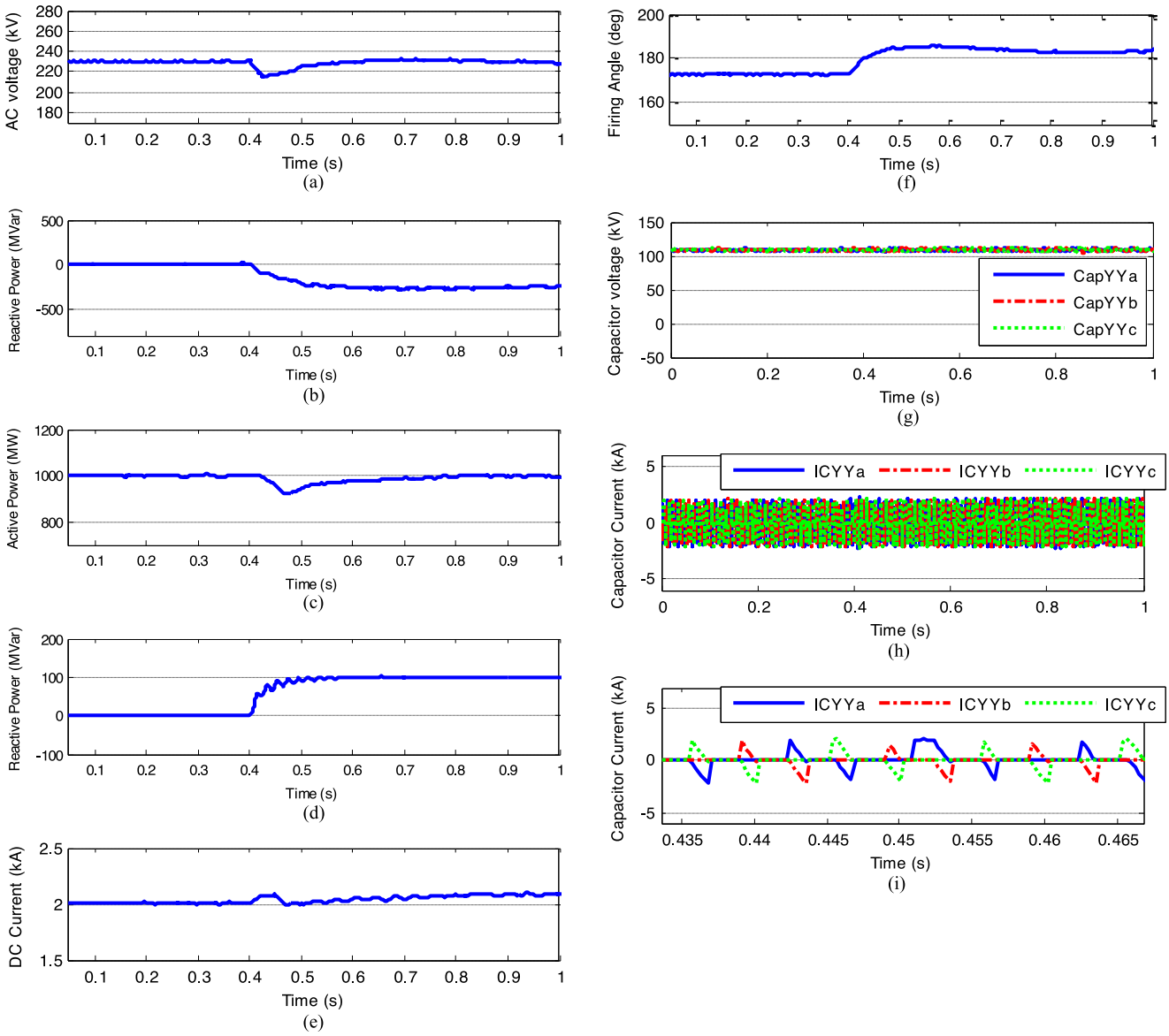

Fig. 14. System responses with large inductive load switching. (a) Inverter AC bus voltage. (b) Inverter reactive power consumption. (c) Active power transfer. (d) Induction machine reactive power. (e) DC current. (f) Inverter firing angle. (g) Capacitor voltages (CapYYa, CapYYb, CapYYc). (h) Capacitor currents for CapYYa, CapYYb and CapYYc. (i) Zoomed in version of capacitor currents.

and the inverter side of the benchmark system is controlling the extinction angle. The rest of the system is left unchanged and all the related system parameters are obtained from [1]. Both the systems shown in Fig. 16(a) and (b) are modelled in RTDS including the detailed models for all the synchronous generators.

In this case study, the reactive power load at bus 9 is increased by 150 MVar at 0.75 s in both the systems to demonstrate the reactive power and AC voltage controllability of the proposed method. Simulation results are shown in Fig. 17. It can be seen from Fig. 17(a) that bus 9 voltage drops in both systems due to the increase of reactive power load. However for the system with the proposed method, the inverter AC voltage controller is able to bring back the bus 9 voltage to its reference value by controlling the inverter to export reactive power as shown in Fig. 17(b) (negative reactive power actually indicates that the inverter is exporting reactive power). On the other hand, as also shown in Fig. 17(b), the reactive power consumption of inverter of the benchmark system stays at around the same value due to the control of extinction angle. Furthermore it can be seen from Fig. 17(c) that the rotor speed difference between G1 and G3 is smaller for the case using the proposed method, especially the magnitude of first swing is minimized

D. *Comparison With HVDC With SVC*

As a comparison to the proposed method, SVC is added to the inverter side of the HVDC benchmark system to control the inverter AC voltage. The single-line diagram of the system is shown in Fig. 18. It can be seen from Fig. 18 that the SVC

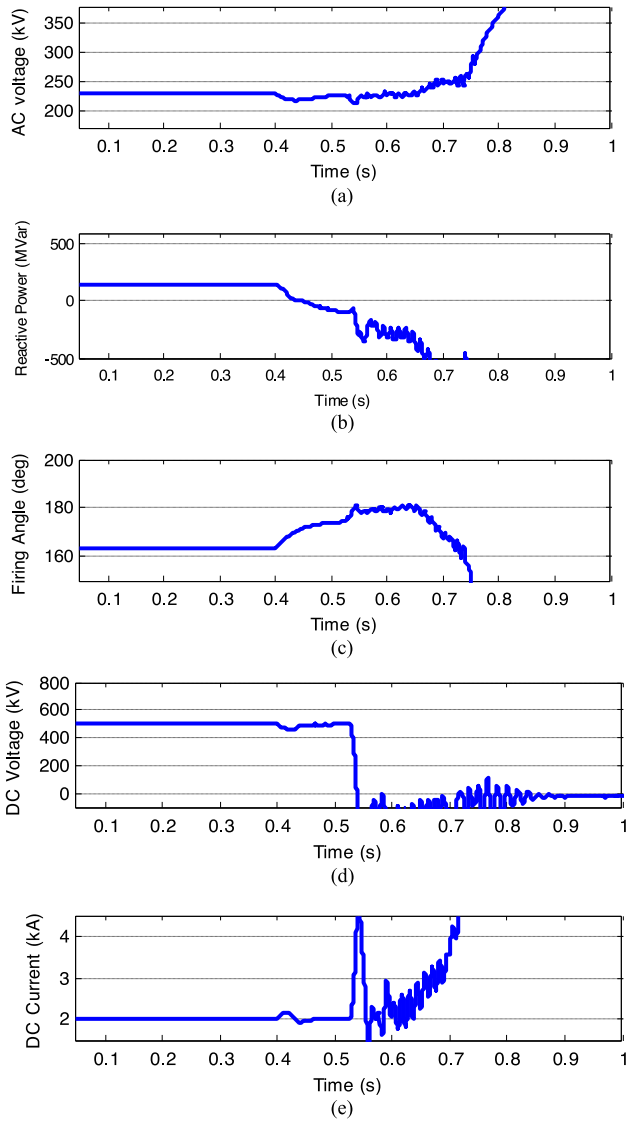

Fig. 15. System responses of CCC HVDC with large inductive load switching. (a) Inverter AC bus voltage. (b) Inverter reactive power consumption. (c) Inverter firing angle. (d) DC voltage. (e) DC current.

being modelled consists of one 117 MVar thyristor controlled reactor (TCR) bank and three 91 MVar thyristor switched capacitor (TSC) banks which are denoted as TSC1, TSC2 and TSC3. They are connected to the secondary side of a 230 kV/8.66 kV coupling transformer. Switching in of the TSCs allows a discrete variation of the reactive power output, whereas TCR allows a continuous variation of its reactive power absorption by controlling its firing angle.

Simulation studies of a step increase in the reactive power load at the inverter AC bus are carried out. In the first case, step increase of 150 MVar of the reactive load is simulated at the inverter AC bus in both the proposed system and the benchmark system with SVC. In the proposed system, the inverter side is controlling the AC voltage and in the benchmark system with SVC, TCR and TSC1 are initially on with zero net reactive power output. Simulation results are shown in Fig. 19. It can be seen from Fig. 19(a) that although the AC voltage is brought

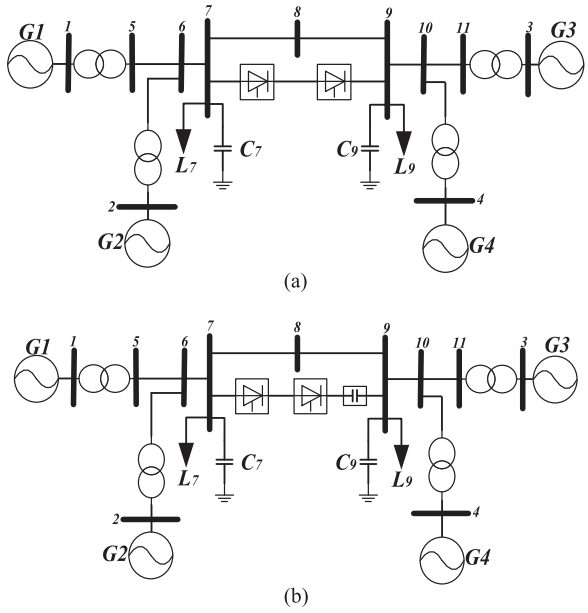

Fig. 16. Single-line diagrams of the two-area four-machine system. (a) Modified four-machine two-area system with the CIGRE Benchmark LCC HVDC. (b) Modified four-machine two-area system using LCC HVDC system with controllable capacitors.

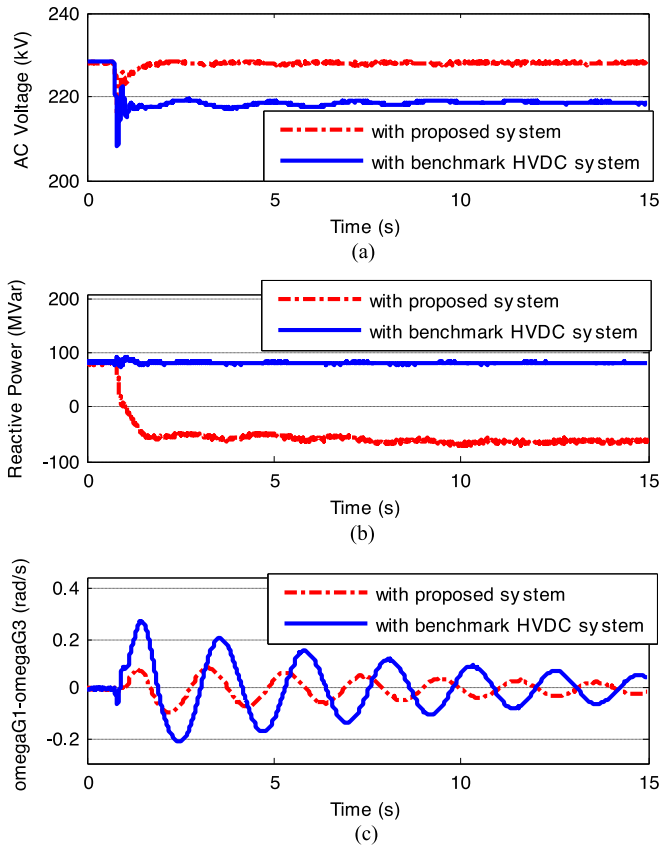

Fig. 17. Simulation results for an increase of reactive power load at bus 9. (a) Bus 9 AC voltage. (b) Inverter reactive power consumption. (c) Rotor speed difference between generator G1 and generator G3.

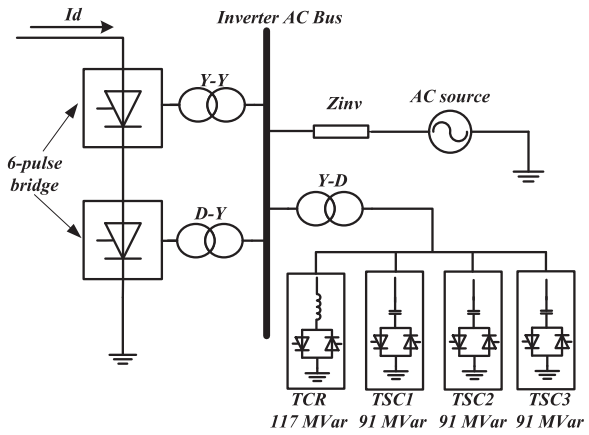

Fig. 18. HVDC benchmark system with SVC.

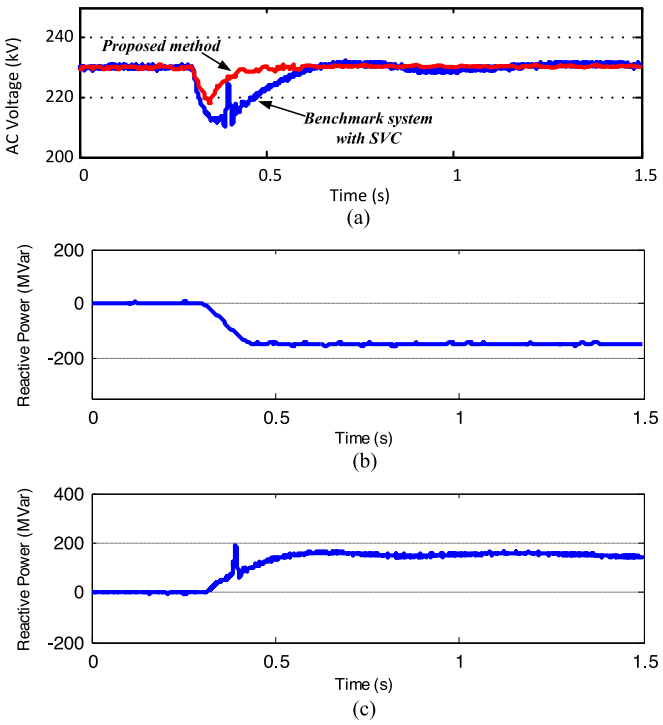

Fig. 19. Simulation results of 150 MVar step reactive power load change. (a) Inverter AC voltages. (b) Inverter reactive power consumption in the proposed system. (c) SVC reactive power output.

back to the reference value in both cases, the response of SVC is slower than that of the proposed controller. The reason is that as the inverter AC bus voltage drops, the inverter extinction angle controller in the benchmark system will advance the firing angle. So the reactive power consumption of the inverter is increased rather than decreased, and this leads to a slower voltage recovery. For the proposed method, the reactive power support is coming from the inverter itself as shown in Fig. 19(b), hence a faster recovery is achieved. Fig. 19(c) shows the reactive power output from SVC where a positive value indicates that the SVC is exporting reactive power. The sudden increase of reactive power in Fig. 19(c) is due to the switching in of TSC2.

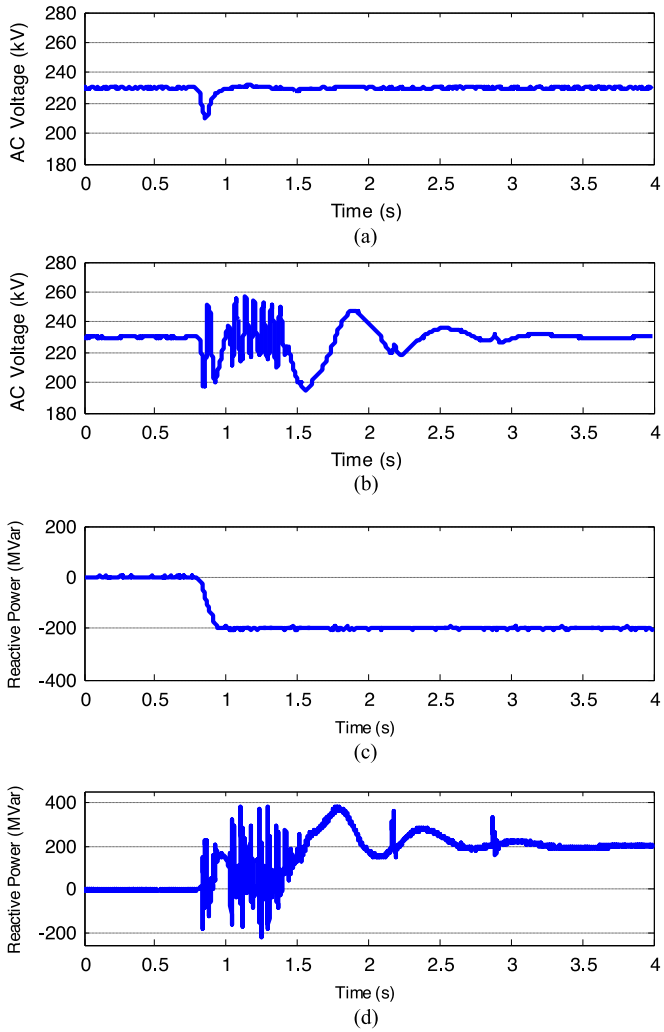

Fig. 20. Simulation results of 200 MVar reactive power load change. (a) Inverter AC voltage in the proposed system. (b) Inverter AC voltage in the benchmark system with SVC. (c) Inverter reactive power consumption in the proposed system. (d) SVC reactive power output.

In the second case study, the magnitude of the step increase becomes 200 MVar and simulation results are shown in Fig. 20. It can be seen from Fig. 20(a) that the AC voltage is successfully controlled at the reference value using the proposed method. The 200 MVar of reactive power load is compensated by the increase of the inverter reactive power export as shown in Fig. 20(c). However for the system with SVC, commutation failure happens due to the larger AC voltage drop and it takes a longer time for the voltage to recover as shown in Fig. 20(b). During the recovery process, large variations of the inverter AC voltage leads to multiple switching actions of TSCs which can be observed from Fig. 20(d).

VI. Conclusion

This paper has investigated and demonstrated the reactive power and voltage control capability of LCC HVDC system with controllable capacitors. The reactive power control and voltage control at the inverter side of the LCC HVDC system

with controllable capacitors have been proposed and associated controllers have been implemented. In connection with the reactive power control or voltage control, active power control at the rectifier side is desirable and such a control has been adopted in this paper.

Detailed mathematical analysis has been carried out and it indicated that if the capacitor voltage level is appropriately chosen, the system is able to achieve zero steady-state reactive power consumption. Hence the size of capacitor banks can be significantly reduced, which leads to considerable cost savings. To further exploit the reactive power controllability, the AC voltage controller is designed to control the inverter AC voltage by the converter itself. Simulation studies and comparisons with CCC HVDC and LCC HVDC with SVC have been carried out using RTDS, and verified the HVDC system's effective reactive power and voltage control capability using the approach proposed. The system's ability of operating under negative extinction angle has been utilized to achieve a wide range of reactive power control and, in particular, the ability of exporting reactive power to the AC system.

REFERENCES

[1] P. Kundur, *Power System Stability and Control*. New York, NY, USA: McGraw-Hill, 1994.

[2] R. P. Burgess, J. D. Ainsworth, H. L. Thanawala, M. Jain, and R. Burton, "Voltage/var control at McNeill back-to-back HVDC converter station," CIGRE Session 14-104, 1990.

[3] B. Andersen, D. Monkhouse, and R. Whitehouse, "Commissioning the 1000MW back to back HVDC link at Chandrapur, India," CIGRE Paper 14-114, 1998.

[4] Y. Zhuang, R. W. Menzies, O. B. Nayak, and H. M. Turanli, "Dynamic performance of a STATCON at an HVDC inverter feeding a very weak AC system," *IEEE Trans. Power Del.*, vol. 11, no. 2, pp. 958–964, Apr. 1996.

[5] O. B. Nayak, A. M. Gole, D. G. Chapman, and J. B. Davies, "Dynamic performance of static and synchronous compensators at an HVDC inverter bus in a very weak AC system," *IEEE Trans. Power Syst.*, vol. 9, no. 3, pp. 1350–1358, Aug. 1994.

[6] M. De Oliveira, M. Poloujadoff, A. Le Du, and P. G. Therond, "Supply of an entirely passive AC system through an HVDC link," *Int. J. Electr. Power Energy Syst.*, vol. 16, pp. 111–116, 1994.

[7] J. W. Feltes, B. D. Gemmell, and D. Retzmann, "From smart grid to super grid: Solutions with HVDC and FACTS for grid access of renewable energy sources," in *Proc. IEEE Power & Energy Society General Meeting*, 2011, pp. 1–6.

[8] S. V. Bozhko, R. Blasco-Gimenez, L. Risheng, J. C. Clare, and G. M. Asher, "Control of offshore DFIG-based wind farm grid with line-commutated HVDC connection," *IEEE Trans. Energy Convers.*, vol. 22, no. 1, pp. 71–78, Mar. 2007.

[9] L. Yong, L. Longfu, C. Rehtanz, S. Ruberg, and L. Fusheng, "Realization of reactive power compensation near the LCC-HVDC converter bridges by means of an inductive filtering method," *IEEE Trans. Power Electron.*, vol. 27, no. 9, pp. 3908–3923, Sep. 2012.

[10] D. Hanguang, W. Yuhong, L. Xingyuan, D. Hongqiang, and M. Zhiqiang, "Characteristic analysis of reactive power compensation device at HVDC converter station," in *Proc. Power Energy Eng. Conf.*, 2012, pp. 1–5.

[11] M. Yadav and K. Manohar, "ANN based SPVC for reactive power compensation of LCC HVDC for offshore wind power transmission," in *Proc. Int. Conf. Electr., Electron., Signals, Commun. Optim.*, 2015, pp. 1–6.

[12] R. Blasco-Gimenez, N. Aparicio, S. Ano-Villalba, and S. Bernal-Perez, "LCC-HVDC connection of offshore wind farms with reduced filter banks," *IEEE Trans. Ind. Electron.*, vol. 60, no. 6, pp. 2372–2380, Jun. 2013.

[13] D. Renchang, M. D. Hwang, Q. Wei, W. Weiguo, L. Xiaopeng, and X. Yan, "EMS experience of reactive power control for LCC based HVDC system," in *Proc. IEEE Power & Energy Soc. General Meeting*, 2015, pp. 1–5.

[14] Y. Xiaoran, Y. Fenyan, F. Xiazhou, and X. Zheng, "Principle and algorithm of reactive power management for LCC-based parallel MTDC transmission system," in *Proc. Int. Conf. Power Syst. Technol.*, 2014, pp. 2265–2271.

[15] S. Oh, G. Jang, S. Moon, Y. Jeon, and J. Choo, "Optimal reactive power compensation scheme for the Jeju-Haenam HVDC system," in *Proc. IEEE/PES Transm. Distrib. Conf. Exhib.*, 2002, vol. 3, pp. 1922–1925.

[16] G. Balzer and H. Muller, "Capacitor commutated converters for high power HVDC transmission," in *Proc. 7th Int. Conf. AC-DC Power Transm.*, 2001, pp. 60–65.

[17] A. M. Gole and M. Meisingset, "Capacitor commutated converters for long-cable HVDC transmission," *Power Eng. J.*, vol. 16, pp. 129–134, 2002.

[18] J. Reeve, J. A. Baron, and G. A. Hanley, "A technical assessment of artificial commutation of HVDC converters with series capacitors," *IEEE Trans. Power App. Syst.*, vol. PAS-87, no. 10, pp. 1830–1840, Oct. 1968.

[19] M. Meisingset and A. M. Gole, "Control of capacitor commutated converters in long cable HVDC-transmission," in Proc. *IEEE Power Eng. Soc. Winter Meeting*, 2001, vol. 2, pp. 962–967.

[20] T. Jonsson and P. Bjorklund, "Capacitor commutated converters for HVDC," in *Proc. Stockholm Power Tech: Power Electron*., 1995, pp. 44–51.

[21] D. Jovcic, "Thyristor-based HVDC with forced commutation," *IEEE Trans. Power Del.*, vol. 22, no. 1, pp. 557–564, Jan. 2007.

[22] Y. Xue, X. P. Zhang, and C. Yang, "Elimination of commutation failures of LCC HVDC system with controllable capacitors," *IEEE Trans. Power Syst.*, vol. 31, no. 4, pp. 3289–3299, Jul. 2016.

[23] M. Szechtman, T. Wess, and C. V. Thio, "A benchmark model for HVDC system studies," in *Proc. Int. Conf. AC DC Power Transm.*, 1991, pp. 374–378.

[24] K. Sadek, M. Pereira, D. P. Brandt, A. M. Gole, and A. Daneshpooy, "Capacitor commutated converter circuit configurations for DC transmission," *IEEE Trans. Power Del.*, vol. 13, no. 4, pp. 1257–1264, Oct. 1998.

[25] M. Meisingset and A. M. Gole, "A comparison of conventional and capacitor commutated converters based on steady-state and dynamic considerations," in *Proc. 7th Int. Conf. AC-DC Power Transm.*, 2001, pp. 49–54.

Ying Xue received the B.Eng. and Ph.D. degrees in electrical engineering from the University of Birmingham, Birmingham, U.K., in 2012 and 2016, respectively. His main research interest includes modeling and control of HVDC and FACTS.

Xiao-Ping Zhang (M'95–SM'06) is currently a Professor in Electrical Power Systems at the University of Birmingham, Birmingham, U.K., and he is also the Director of the Smart Grid of Birmingham Energy Institute. Before joining the University of Birmingham, he was an Associate Professor in the School of Engineering at the University of Warwick, Coventry, U.K. From 1998 to 1999, he visits the University of Manchester Institute of Science and Technology. From 1999 to 2000, he was an Alexander-von-Humboldt Research Fellow with the University of Dortmund, Germany. He worked at China State Grid EPRI on EMS/DMS advanced application software research and development between 1993 and 1998. He is the co-author of the monograph *Flexible AC Transmission Systems: Modeling and Control* (1st, 2nd, ed. New York, NY, USA: Springer-Verlag, 2006, 2012). He is also the co-author of the book entitled *Restructured Electric Power Systems: Analysis of Electricity Markets with Equilibrium Models* (Piscataway, NJ, USA: IEEE Press/Wiley, 2010). Internationally, he pioneered the concept of "Energy Union" and "UK's Energy Valley."